Applied Catalysis B: Environmental 162 (2015) 593–601

Contents lists available at ScienceDirect

Applied Catalysis B: Environmental

journal homepage: www.elsevier.com/locate/apcatb

Preparation and evaluation of a highly stable palladium yttrium platinum core–shell–shell structure catalyst for oxygen reduction reactions

Xiaoteng Liu*, Eileen H. Yu, Keith Scott

Chemical Engineering and Advanced Materials, Merz Court, Newcastle University, Newcastle upon Tyne, NE1 7RU, United Kingdom

ARTICLE INFO

Article history:
Received 6 May 2014
Received in revised form 3 July 2014
Accepted 19 July 2014
Available online 29 July 2014

Keywords:
Fuel cell
Catalyst
Durability
Core–shell–shell structure
Oxygen reduction reaction

ABSTRACT

A core–shell–shell structure Pd–Y–Pt/C catalyst was prepared using a controlled surface reaction method. The structure was confirmed by X-ray photoelectron spectroscopy (XPS) and energy dispersive X-ray (EDX) techniques. Nano-scale yttrium was formed as a shell located as the middle layer of the catalyst. Electrochemical evaluation of the Pd–Y–Pt/C with less than 7% of Pt showed an improved performance toward oxygen reduction reaction (ORR) compared to Pt/C (20 wt.% Pt). Accelerated degradation tests (ADT) indicated that the addition of Y improved catalyst stability compared to Pt/C and Pd–Pt/C core–shell catalysts under various experimental conditions. This was due to the Y middle layer created approximate half-filled metal–metal d bond between Pt (or Pd) and Y. This catalyst utilized the core–shell–shell structure to minimize the Pt usage, and Y middle shell to improve stability.

1. Introduction

Catalyst is the most important factor which governs the performance of polymer electrolyte membrane fuel cells (PEMFCs). It has been extensively studied in the past decades in terms of increasing the catalyst durability and reducing the cost. Carbon supported Pt nano-particle catalyst is recognized as the best candidate for oxygen reduction reactions (ORRs). It has been reported that the fuel cell suffers from power loss after a certain period running due to the degradation of the cathode catalyst [1–3]. This degradation of catalyst is caused by sintering of the Pt particles [4,5] and corrosion of the carbon support [6,7]. In terms of increasing the activity and durability on cathode side, Pt based alloys were widely studied. Among the Pt–M bimetallic catalysts, Jeon et al. [8] found that Pt–Y/C has 20% higher mass activity and 65% higher specific activity than comparable Pt/C catalyst. Greeley et al. [9] reported that Pt alloyed with early transition metals such as Sc or Y ORR catalysts are the most stable Pt based binary alloys using density functional theory calculations, their electrochemical measurements showed that the activity of polycrystalline Pt_3–Sc and Pt_3–Y electrodes is enhanced relative to pure Pt by a factor of 1.5–1.8 and 6–10, respectively, in the range of 0.9–0.87 V. Researchers also found that Pd based alloys can be a good candidate to replace Pt for the purpose of cost reduction as well as retain a comparable activity to Pt/C catalysts [10–12]. Both Greeley et al. [9] and Seo et al. [13] found that Pd_3–Y/C showed increased ORR activity and stability than Pt/C catalyst.

Core–shell structure nanoparticle catalyst has recently become the research trend, because it reduces the usage of the noble metal when used as shell material as well as retains similar or prior catalytic activity compared to bulk alloy catalysts. Zhang et al. [12] and Sasaki et al. [14] prepared Pd–Pt core–shell structure catalyst using different preparation methods, and both catalysts showed an increased ORR activity, durability and mass activity comparing with Pt/C commercial catalysts. A controlled surface reaction (CSR) method for core–shell catalysts preparation was previously reported by Crabb et al. [15,16], this method utilizes the reaction between an organometallic compound and the core metal surface in a hydrogen environment, and the surface composition was well controlled. It also has the advantage of forming an uniform shell of the second metal on the surface of the core material.

In this present work, Pd–Y–Pt/C core–shell–shell structure catalysts were synthesized using yttrium(III) acetylacetonate hydrate and platinum(II) acetylacetonate in a hydrogen environment to produce Pd as the core, Y as the middle shell on Pd particles and Pt as the outer shell. Meanwhile, a Pd–Pt/C core–shell structure catalyst was also included as comparison.

* Corresponding author. Tel.: +44 191 222 5745.
E-mail address: xiaoteng.liu@ncl.ac.uk (X. Liu).

http://dx.doi.org/10.1016/j.apcatb.2014.07.038

2. Experimental

2.1. Materials and chemicals

Vulcan XC-72R carbon powder was purchased from Cabot Corporation (USA). All other chemicals, *ca.*, ammonium tetrachloropalladate(II) ($(NH_4)_2PdCl_4$), yttrium(III) acetylacetonate hydrate ($Y(acac)_3$), platinum(II) acetylacetonate ($Pt(acac)_2$); Nafion 117 solution (5%), sulfuric acid (98%), potassium hydroxide (85%), hydrogen peroxide (30%), sodium hydroxide (97%) and ethanol (99.8%) were purchased from Sigma–Aldrich. Millipore water with 18 MU cm resistivity was used in the experiments.

2.2. Preparation of carbon supported Pt–Y–Pd/C catalyst

The core–shell–shell structure Pd–Y–Pt/C catalyst was prepared in two steps. Firstly, we prepared a 20 wt.% loading of Pd supported on carbon catalyst using polyol method. 500 mg of Vulcan XC-72R carbon powder was dispersed in 150 ml of ethanol in a two neck round flask and the mixture was ultrasonically mixed for 30 min then stirred using a magnetic bar under nitrogen atmosphere for 1 h. 334.0 mg of $(NH_4)_2PdCl_4$ was dissolved in 50 ml de-ionized water and added drop wisely to the mixture. After 1 h stirring, the pH value of this mixture was measured with a Jenway 3310 pH meter and adjusted to 11 by drop wise addition of 2 M NaOH solution. The mixture was refluxed at 75 °C for 12 h under a nitrogen atmosphere. The resultant Pd/C catalyst was washed several times with ethanol and de-ionized water and then dried at 80 °C in a hot air oven.

The second step was to synthesize approximately 1.5 monolayer (ML) equivalence of Y and Pt core–shell–shell Pd–Y–Pt/C catalyst using a controlled surface reaction method [16]. The dispersion of Pd/C was 18.0% which was calculated from the electrochemical surface area (ECSA) in half cell electrochemical testing detailed in Section 2.4, and confirmed with the average particle size (from TEM) and dispersion relationship [17,18]. 1.5 ML coverage was employed to provide a reservoir large enough to enable the Y and Pt formation of particles in which a greater fraction of each particle will consist of the Pd–Y–Pt trimetallic catalyst, *i.e.* yielding particles with a smaller Pd core. Briefly, 500 mg of 20 wt.% Pd/C was reduced with H_2 at 200 °C for 30 min in a three neck round flask reactor. 65.3 mg of $Y(acac)_3$ was dissolved in 100 ml toluene and loaded into a dropping funnel, connected to the reactor. After purging with N_2 gas, the solution was transferred into the reactor at room temperature. After mixing for 2 h the temperature was increased up to 90 °C and maintained for 24 h under pure H_2. This experimental condition allows H_2 to adsorb onto the Pd surface to form Pd–H_{ads}, ideally each H_2 occupies 2 Pd atoms. $Y(acac)_3$ reacts with Pd–H_{ads} by forming Pd–Y and releasing the $C_5H_8O_2$. Then the surface of Pd particles is homogenously covered by Y. The mechanism of controlled surface reaction can be explained in the following formulas [19]:

$$Pd + H_2 \rightarrow Pd\text{–}H_{ads}$$

$$Pd\text{–}H_{ads} + Y\text{–}R_n \rightarrow Pd\text{–}Y + nH\text{–}R$$

Then the content was cooled down to room temperature under N_2. 66.5 mg of $Pt(acac)_2$ was dissolved in 100 ml toluene and loaded into the dropping funnel, then added into the same reactor after purging with N_2 at room temperature. The content then, again, heated up to 90 °C and the reaction was carried out under H_2 for 4 h to allow Pt deposit onto the Y surface. The contents of the reactor were filtered, washed, dried and reduced again with H_2 at 250 °C for 2 h, a small amount of this catalyst was heat treated at 350 °C for 2 h to check the function of Y against the heat treatment condition. NaOH solution was added to the filtrates in terms of checking any unreacted Y or Pt precursors. The resulting trimetallic catalyst had a composition of 18.1 wt.% Pd, 3.0 wt.% Y and 6.6 wt.% Pt. A 20% Pt/C catalyst was also prepared using the same polyol method from chloroplatinic acid as comparison.

2.3. Characterizations

X-ray photoelectron spectroscopy (XPS) analysis was used to elucidate the electronic structures and composition of the Pd–Y–Pt/C and Pd–Pt/C nanoparticles. XPS analysis was performed with a Kratos Axis Nova spectrometer. The catalyst was fixed on the support using a copper double-sided adhesive conducting tape and then evacuated at room temperature. The spectra were excited by the monochromatized Al Ka source (1486.6 eV) run at 15 kV and 10 mA. For the individual peak regions a pass energy of 20 eV was used. Survey spectrum was measured at 160 eV pass energy. Analyses of the peaks were performed with the CasaXPS software after Shirley background subtraction. The peaks were fitted using an asymmetric Gaussian–Lorentzian sum function with the constraint that all the peaks display the same asymmetry and Gaussian/Lorentzian ratio. The binding energies were lined up with respect to the C 1s peak at 284.6 eV. High resolution transmission electron microscopy (HRTEM) was employed to determine the morphology of the catalysts, energy dispersive X-ray (EDX) fitted in HRTEM was used to analyze the structure of core–shell–shell nanoparticles, both line and mapping scans was performed to identity the structure of Pt, Y and Pd elements. The HRTEM/EDX analysis was performed at Leeds Electron Microscopy and Spectroscopy (LEMAS) Center. The instrument was FEI Tecnai TF20 FEGTEM Field emission gun TEM/STEM fitted with HAADF detector, and Oxford Instruments INCA 350 EDX system/80 mm X-Max SDD detector and Gatan Orius SC600A CCD camera.

2.4. Electrochemical evaluation

Half cell electrochemical evaluations were conducted using a BASi RRDE-3A package which consists of a rotating ring disk electrode (RRDE) apparatus, a glass cell vial (100 ml), an Ag/AgCl reference electrode, a 7.5 cm long Pt wire with 0.5 mm diameter and RRDE tip. The RRDE tip consisted of a glassy carbon disk with a surface area of 0.1256 cm^2 and platinum ring surface area of 0.1884 cm^2. The data were recorded using an AutoLab PGSTAT30 potentiostat/galvanostat with GPES software. The potential reported in this study are referred to the reference hydrogen electrode (RHE). The loading of catalyst deposited on the GC disk was 0.5 mg cm^{-2}. The ink was prepared by ultrasonically mixing the catalysts and 5.0 wt.% Nafion ionomer in ethanol. A required amount of the catalyst slurry was carefully dropped on glassy carbon surface and allowed to dry at room temperature for 15 min to obtain a uniform catalyst film. The cyclic voltammograms (CV) were recorded at 0.2 V s^{-1} between 0 and 1.2 V *vs.* RHE, the ECSA of reduction peak which is between potential 1.0–0.4 V *vs.* RHE at cathodic sweep was considered as the active surface area of the catalysts. The charge related to a monolayer of double banded oxygen pieces reduction was 420 μC cm^{-2}. The dispersion value of Pd–C catalyst (for preparation of Pd–Y–Pt/C catalyst) was calculated using this method to find out the active amount of Pd atoms out of the total Pd atoms in certain amount of Pd/C catalyst. After the initial measurement, the electrodes were scanned 20,000 times under the same condition as ADT test. The electrolytes were 0.5 M H_2SO_4 solution saturated with N_2 for the CV and potential cycling ADT test. ORR profile was analyzed using the same electrode in O_2 saturated 0.5 M H_2SO_4, linear scan voltammetry (LSV) was recorded from 1.0 to 0.5 V *vs.* RHE against the increasing rotation speeds—400, 900, 1600 and 2500 rpm. RRDE study was carried

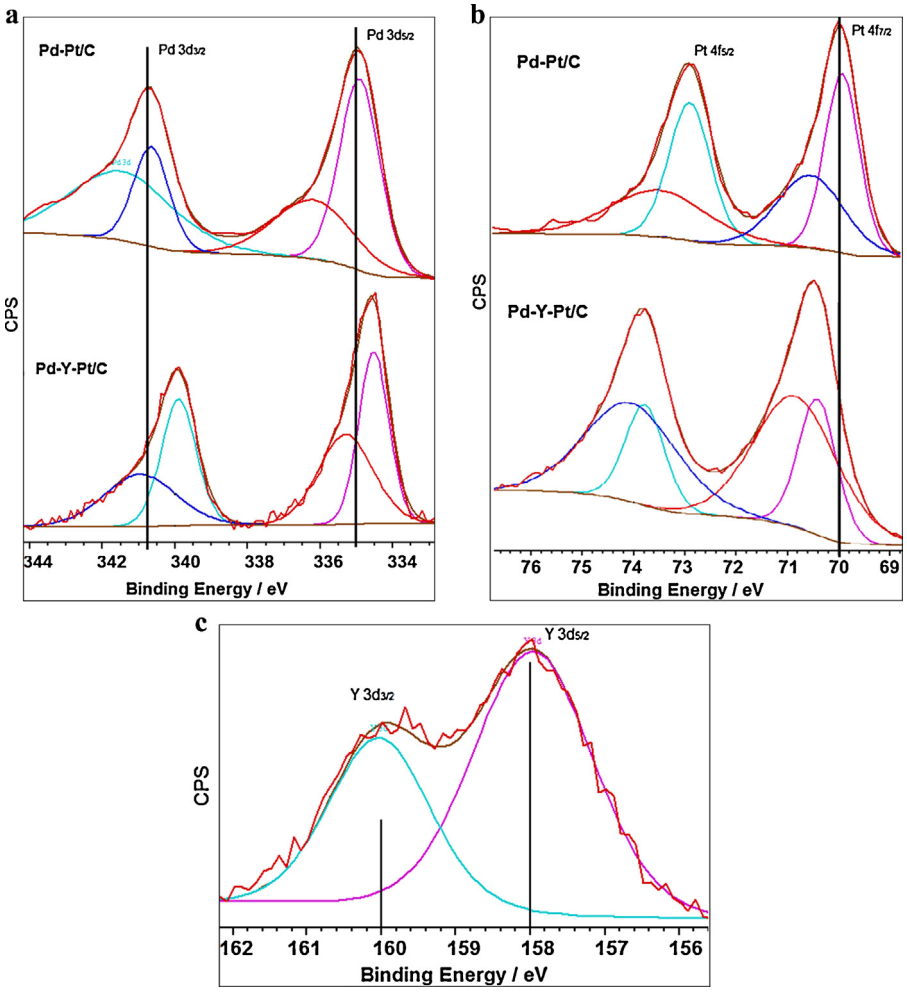

Fig. 1. XPS (a) Pd 3d, (b) Pt 4f and (c) Y 3d spectra of Pd–Y–Pt/C and Pd–Pt/C catalysts.

out to check the peroxide during O_2 reduction, the electrode was scanned between the potential 1.0 and 0 V *vs.* RHE in O_2 saturated 0.5 M H_2SO_4, the potential applied on the ring was 1.2 V. The scan rate for both ORR tests was 0.005 V s^{-1}. All half-cell experiment was carried out at room temperature.

3. Results and discussion

3.1. Composition analysis and structure characterizations

XPS analyses were used to elucidate the electronic structures and composition of the Pd–Y–Pt/C and Pd–Pt/C nanoparticles. Table 1 lists the composition of each element from preparation calculations and XPS analysis. The values from XPS analysis are generally in agreement with the preparation calculation, which means that both Y and Pt were reduced from the precursors. However, XPS indicated slightly higher values of Pt and Pd and lower value of Y, this could be attributed to electronegativity differences, leading to charge transfer from the less electronegative Y to the more-electronegative Pd and Pt [13].

Table 1
Preparation and XPS elementary analysis of Pd–Y–Pt/C and Pd–Pt/C catalysts.

	Pd–Y–Pt/C (% wt.)			Pd–Pt/C (% wt.)	
	Pd	Y	Pt	Pd	Pt
Preparation	18.1	3.0	6.6	18.6	6.8
XPS	18.8	2.4	6.9	19.0	7.0

Fig. 1 shows the XPS (a) Pd 3d, (b) Pt 4f and (c) Y 3d spectra of Pd–Y–Pt/C and Pd–Pt/C catalysts. The binding energy (BE) of the major doublet of Pd–Pt/C in Fig. 1(a) appears at 335.3 eV and 340.5 eV, respectively, and were attributed to the presence of metallic Pd (0) [20,21]. Another doublet at 336.4 and 341.3 eV, respectively, was attributed to an oxidation state similar to that of Pd (II) [13,21]. All these peak positions shifted more negtively than Pd/C monometallic catalyst, because of the presence of Pt and the d–d bond hybridization occurs between two metal elements [13,22]. BEs of Pd–Y–Pt/C had an even further negative shift than Pd–Pt/C, this is likely to attributed to the presence of Y in the catalyst. The effect of Y also observed from the BEs of Pt 4f spectra in Fig. 1(b). All peak positions of Pd–Y–Pt/C were shifted positively when compared with the Pd–Pt/C catalyst. In Fig. 1(c), the Y 3d BEs were observed at 157.9 and 159.8 eV which differ from the metallic Y (156.0 and 158.5 eV) [23], this could result from the low temperature heat treatment condition and the influence of Pt and Pd. There is no peak of Y_xO_y observed from XPS analysis, and we assume that Y in this catalyst present in zero-valent or oxidant state Y is lower than detective level.

Fig. 2 shows the TEM image of Pd–Y–Pt/C catalyst heat treated at 250 °C. Spherical particles were mostly homogenously deposited on the carbon substrate. Particle size distribution of Pd/C, Pd–Pt/C, Pd–Y–Pt/C heat treated at 250 and 350 °C are presented in Fig. 3. All catalysts have narrow particle size distribution, the average particle

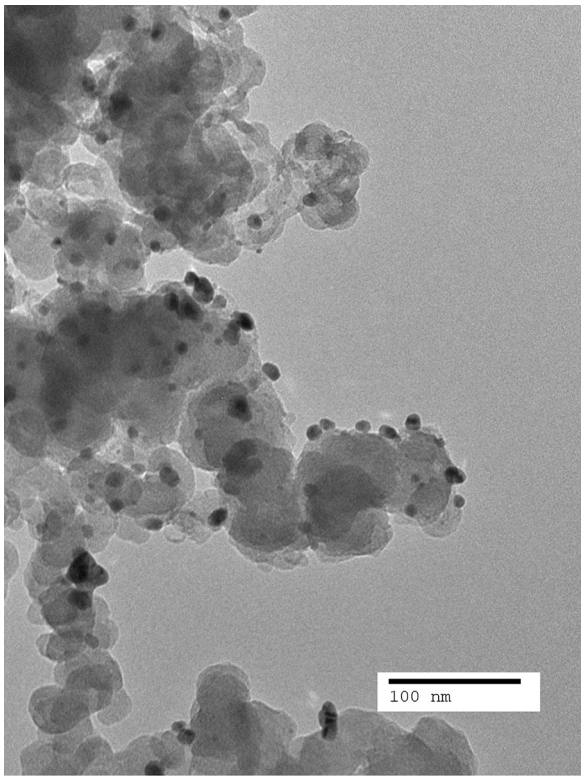

Fig. 2. TEM image of Pd–Y–Pt/C catalyst heat treated at 250 °C.

size of Pd/C is 9.9 nm, and of Pd–Pt/C, Pd–Y–Pt/C heat treated at 250 and 350 °C are 10.4 nm, 10.5 nm and 10.8 nm, respectively. The addition of Pt on Pd gave an increase of 0.48 nm, this minor increase reflected that only atomic layers of Pt was added onto the surface of Pd. Another 0.11 nm increase in average particle size was observed with the addition of Y. The Pd–Y–Pt/C heat treated at 350 °C has 0.29 nm bigger in average particle size which is much smaller than this of Pd based catalysts prepared at similar temperature by other researchers [24–26]. It can be predicted that the Y middle layer could prevent particle size growth with increasing temperatures.

Morphological elements analysis was performed using EDX line scan and confirmed with mapping scan in LEMAS center. This technique allows us to see the location of the Y and Pt as well as the core material Pd. Figs. 4 and 5 show the HAADF, elemental line spectra and mapping profile of Pd, Y and Pt of Pd–Y–Pt/C catalyst as well as the overlaid elemental mapping scan image for single particles. The existence of the 3 elements has been confirmed, it gave the evidence of deposition of Y and Pt from the precursor was successful. The EDX electron beam went along the green line shown in the dark field image in Fig. 4. Spectra (a) indicate the intensity detected by the electron beam went across the particle, it is clear that Pt presents on the outer surface followed by strong Y peaks slightly located inside. Pd mainly composed as the core which covered by Y then Pt. Dark image Fig. 4(b) shows a blurred profile of the particle, because that the particle is slightly burnt by the high energy electron beam after the pervious scan. In Fig. 4(b), the scan went across the edge of the particle, the corresponding spectra indicate a clear core–shell–shell structure, however, each elements were slightly overlapped because the atoms were scattered. EDX mapping scan in Fig. 5 gives complementary detail confirms the core–shell–shell structure. Analysing the particle, Pd was present in the middle as prepared as the core material, Pt is composed as a ring and mainly located on the outer layer of the particles, Y has relatively low level signal strength, however, it can be seen that the Y signal had higher concentration between the Pd core and Pt shell. The core–shell–shell structure was successfully achieved by the controlled surface reaction preparation method. XPS and CV results also gave evidence that Y is covered by Pt rather than exposed on the surface.

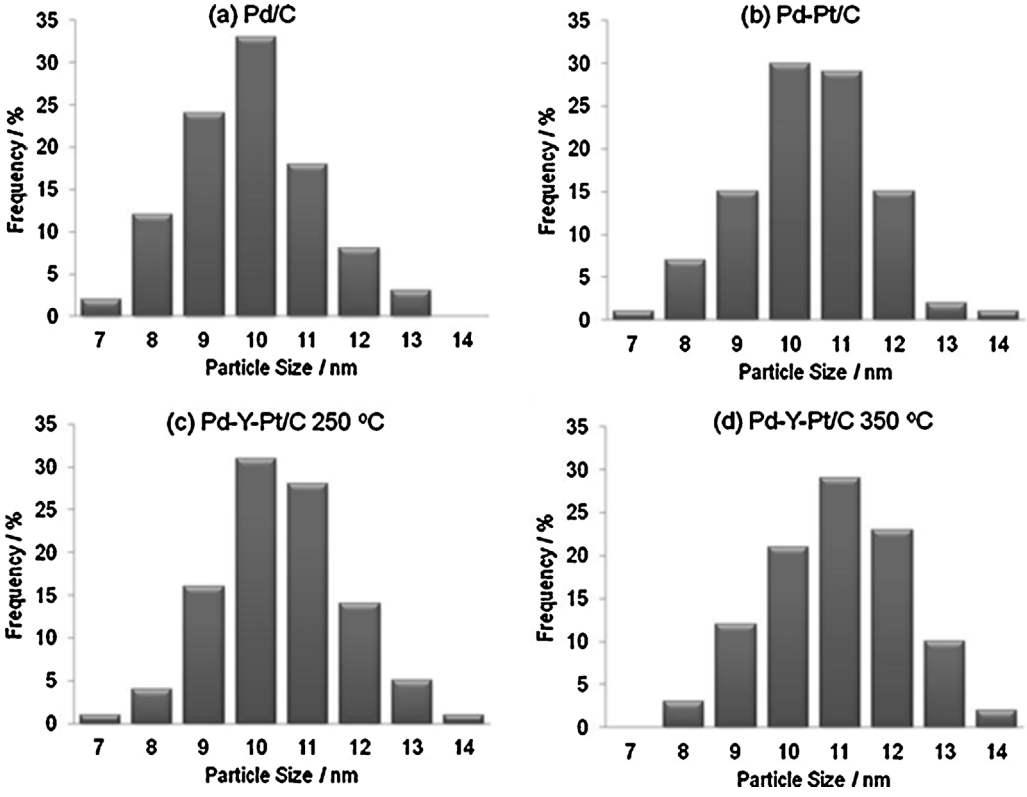

Fig. 3. Particle size distribution of Pd/C, Pd–Pt/C, Pd–Y–Pt/C heat treated at 250 and 350 °C.

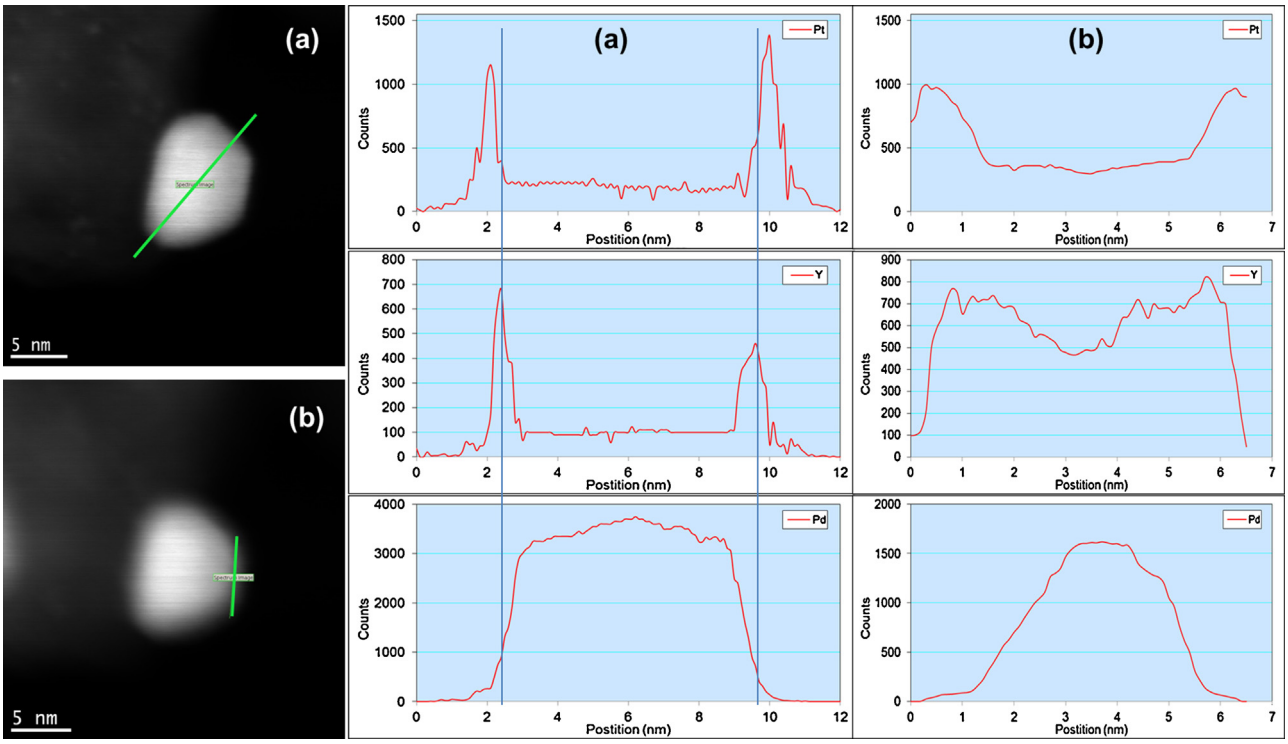

Fig. 4. HAADF image and EDX line scan spectra of Pd, Y and Pt of Pd–Y–Pt/C catalyst.

3.2. Electrochemical evaluation

Cyclic voltammetry (CV) was performed by scanning the electrodes in N_2 saturated 0.5 M H_2SO_4 electrolyte between 0 and 1.2 V *vs.* RHE at room temperature. Fig. 6 shows the cyclic voltammograms of Pd–Y–Pt/C heat treated at 250 °C and 350 °C, Pd–Pt/C and Pt/C catalysts. All catalysts exhibited well-defined hydrogen under-potential deposition (UPD) symmetric response around 0.1–0.2 V *vs.* RHE, and clear surface oxidation/reduction region at potentials higher than 0.6 V *vs.* RHE. Considering the oxide reduction onset potentials appear at around 0.9–1.0 V *vs.* RHE, Pd–Y–Pt/C indicated a onset potential of 1.1 V *vs.* RHE which is higher than 0.9 V *vs.* RHE of Pd/C [10,27,28]. Pd–Y–Pt/C has very similar oxide reduction onset potential to Pt/C, in addition, a sharper single reduction peak was observed, and the maximum peak potential is 0.1 V higher the Pt/C. Similar results also observed and reflect that the Pd surface was covered by Pt of Pd–Pt/C catalyst. In terms of comparing the catalytic activity, the HUPD electrochemical surface area (ECSA) and the electrochemical platinum surface area (EPSA) of Pt/C, Pd–Pt/C and Pd–Y–Pt/C are listed in Table 2. Both Pd–Pt/C and Pd–Y–Pt/C have slightly increased ECSA per mg metal than Pt/C. larger surface area may result from Pt atoms which well dispersed on the surface [15,16]. EPSA reflects the catalytic activity per mg Pt. It is clear that the core–shell structure catalysts indicate dramatic increased EPSA than Pt/C, because of the benefit from the core–shell structure. The electrochemical reaction only occurs on the catalyst surface, so the Pt efficiency has been increased as it only located on the surface of the catalysts. The purpose of including Pd–Y–Pt/C heat-treated at 350 °C is to see the influence of heat treatment temperature when Y involved. Interestingly, with 100 °C higher heat treatment condition, the Pd–Y–Pt/C did not show any reduction in current density, but an increase in current density and a positively shifted onset oxide reduction potential were observed. This could indicate that Y protected the Pd particle growth and influenced the growth of Pt on the surface. The improvement of this aspect will be further investigated in our future work.

Accelerated degradation test (ADT) was performed by scanning the electrodes 20,000 times under the same half-cell condition between 0 and 1.2 V *vs.* RHE. The initial and the 20,000th scans are compared in Fig. 7 for the ADT CVs of Pt/C, Pd/C, Pd–Pt/C and Pd–Y–Pt/C catalysts. A decrease of current density on hydrogen UPD and oxidation/reduction regions was observed on all catalysts. Pd/C has the most intensive degradation due to the dissolution of Pd atoms. Pt/C showed a better stability than Pd/C, however, the Pt atom dissolution and surface structure rearrangement still occurred, the electrochemical surface area (ECSA) of hydrogen oxidation peak at UPD region had a 46% decrease. While the surface of Pd covered by Pt only, the Pt–Pd/C core–shell catalyst showed a similar degradation with a decrease of 32% in ESA. Pd–Y–Pt/C core–shell–shell structure catalyst exhibited even better stability with only 22% decrease in ESA. The results suggested that with a core–shell structure, the Pd–Pt/C catalyst had a better stability which is in agreement with the finding of Zhang et al. [29]. The effect of Y on improving stability of Pd–Y–Pt/C is observed when compared to the result with Pd–Pt/C.

ORR profile was analyzed using the same electrodes in O_2 saturated 0.5 M H_2SO_4, Fig. 8 shows the effect of the RDE rotation speed on the LSV data for Pd–Y–Pd/C catalyst, the rotation speeds was 400, 900, 1600 and 2500 rpm. The LSV curves showed a parallel profile, and the limiting current is gradually increased with increasing rotation speed. The onset potentials of ORR were observed at around 0.95 V *vs.* RHE which is the same to Pt/C monometallic catalyst [28]. The Koutecky–Levich plots at different potentials showed a linear dependence at all potentials (Fig. 9). The linear and the parallel form of these plots usually indicate first-order kinetics with respect to molecular oxygen, although this criterion is not very specific [30]. The number of electrons in the ORR can be calculated from the Koutecky–Levich equation:

$$\frac{1}{i} = \left(\frac{i}{i_k}\right) + \left(\frac{1}{i_f}\right) + \left(\frac{1}{i_d}\right) \quad (1)$$

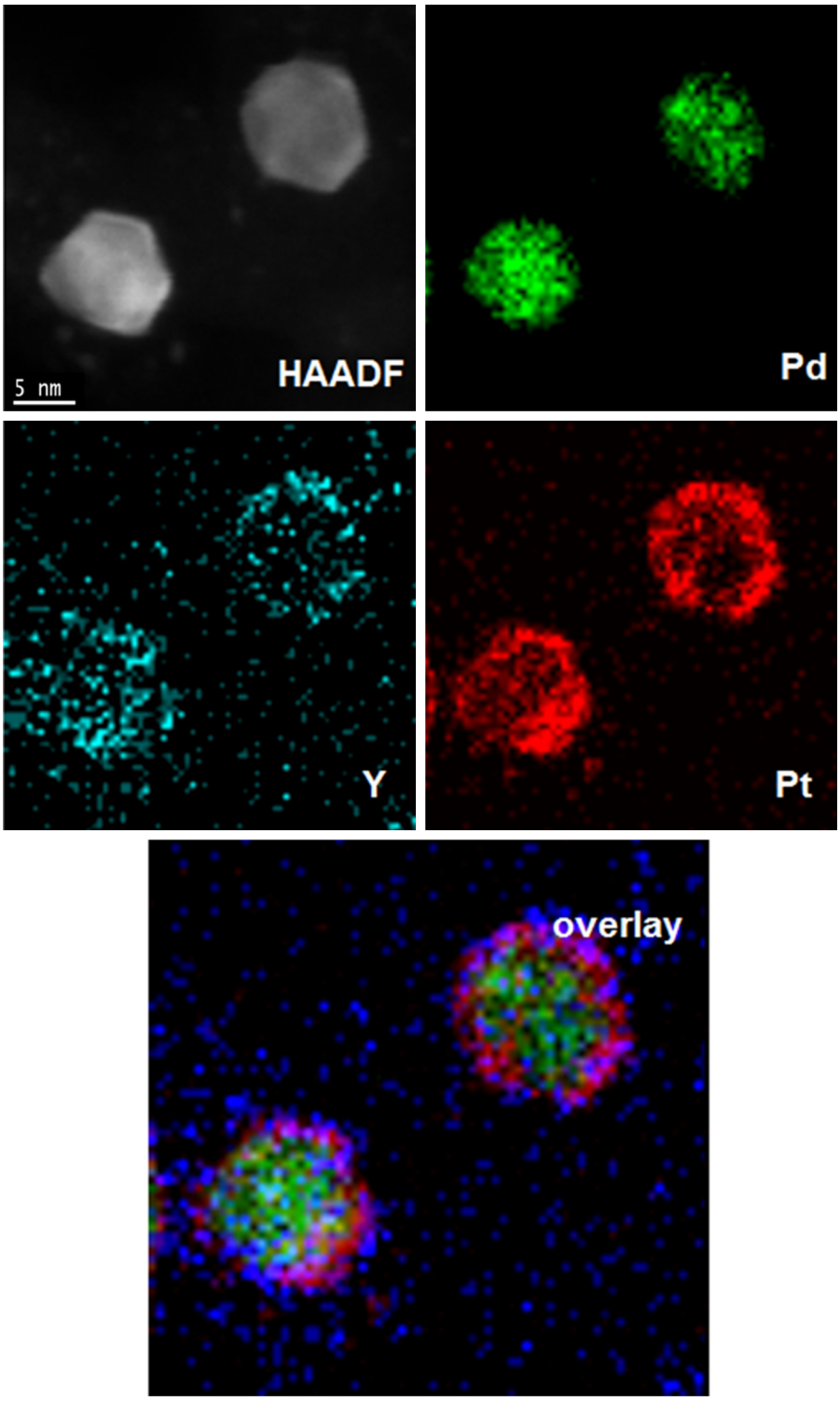

Fig. 5. HAADF, elemental mapping scan of Pd, Y and Pt of Pd–Y–Pt/C catalyst and the overlaid elemental scan image.

Table 2
Electrochemical activity parameters obtained from CV and ORR results for Pt/C, Pd–Pt/C and Pd–Y–Pt/C heat-treated at 250 °C catalysts.

	ECSA ($cm^2\ mg^{-1}_{metal}$)	EPSA ($cm^2\ mg^{-1}_{Pt}$)	I @ 0.8 V *vs.* RHE ($mA\ cm^{-2}$)	Metal mass activity @ 0.8 V *vs.* RHE ($mA\ mg^{-1}$)	Pt mass activity @ 0.8 V *vs.* RHE ($mA\ mg^{-1}_{Pt}$)	n
Pt/C	426	426	2.32	184.7	184.7	3.74
Pd–Pt/C	453	1696	2.14	185.9	696.3	3.67
Pd–Y–Pt/C	481	2021	2.36	187.9	789.8	3.92

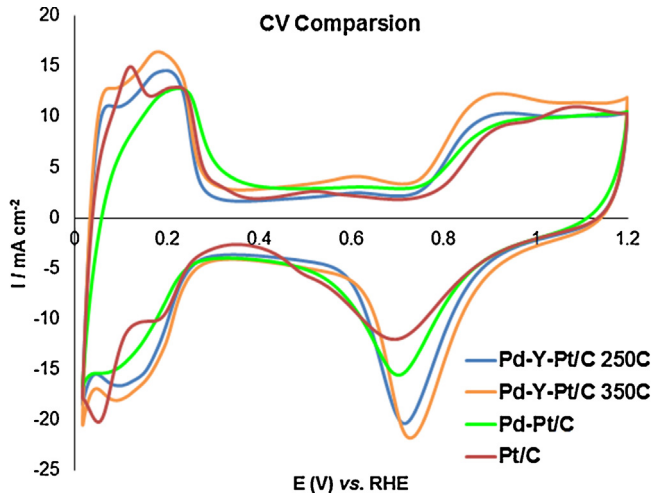

Fig. 6. Cyclic voltammograms of Pd–Y–Pt/C heat treated at 250 °C and 350 °C, Pd–Pt/C and Pt/C catalysts.

Since the amount of Nafion in the electrode is small and the film resistance is sufficiently small (~0.01 $cm^2\ mA^{-1}$), the overall current can be described as:

$$\frac{1}{i} = \left(\frac{i}{i_k}\right) + \left(\frac{1}{i_d}\right) \quad (2)$$

The value for i_d can be represented as

$$i_d = 0.62nFACD^{2/3}\upsilon^{-1/6}\omega^{1/2} \quad (3)$$

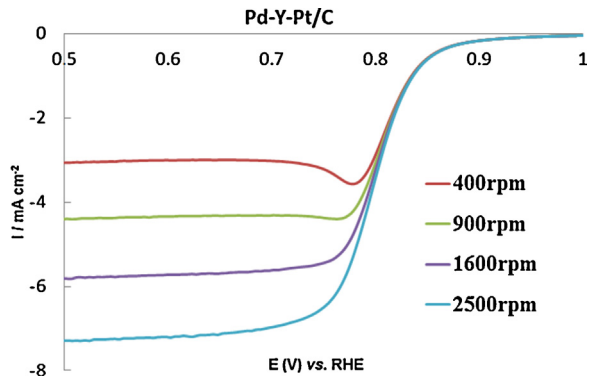

Fig. 8. LSV response with increasing rotation speed for Pd–Y–Pd/C catalyst.

where n is the number of electrons transferred in the reaction, F is the Faraday constant, A is geometric surface area of the electrode, C is the concentration of O_2 in the solution at atmospheric pressure (1.03×10^{-3} M), D is the diffusion coefficient for O_2 ($2.1 \times 10^{-5}\ cm^2\ s^{-1}$), n is the kinematic viscosity ($1.1 \times 10^{-2}\ cm^2\ s^{-1}$) and ω is the electrode rotation rate. From the slops of Koutecky–Levich plots, n value of Pd–Y–Pt/C is presented in Table 2 along with the n values of Pt/C and Pd–Pt/C catalysts. All three catalysts indicated a four-electron reduction of O_2 as the n values are within the range of 3.6–4.0. At 0.8 V *vs.* RHE, the practical operating potential of fuel cell cathode, the current density was measured for the three catalysts at 900 rpm on ORR scans. Metal mass activity and Pt mass activity were calculated using such current density, these values are also listed in Table 2.

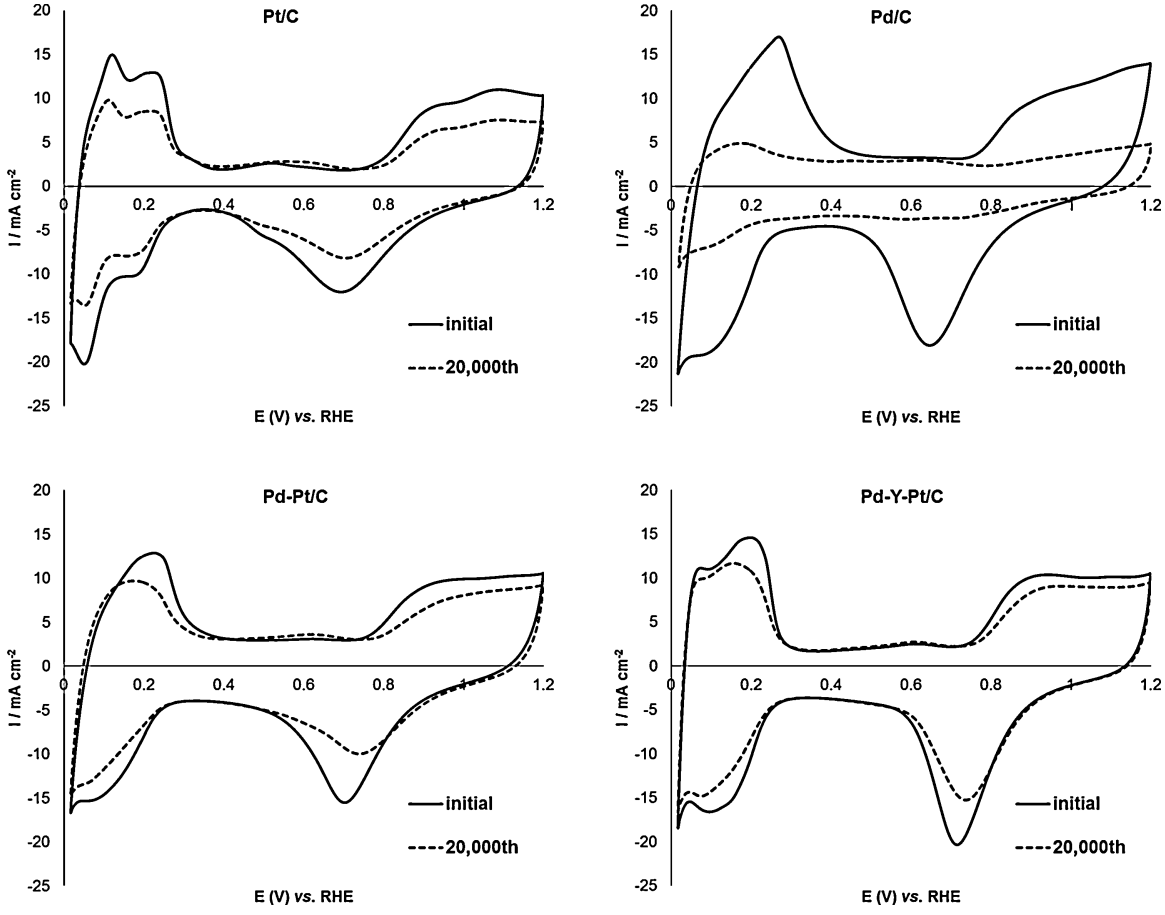

Fig. 7. The ADT CVs of Pt/C, Pd/C, Pd–Pt/C and Pd–Y–Pt/C catalysts.

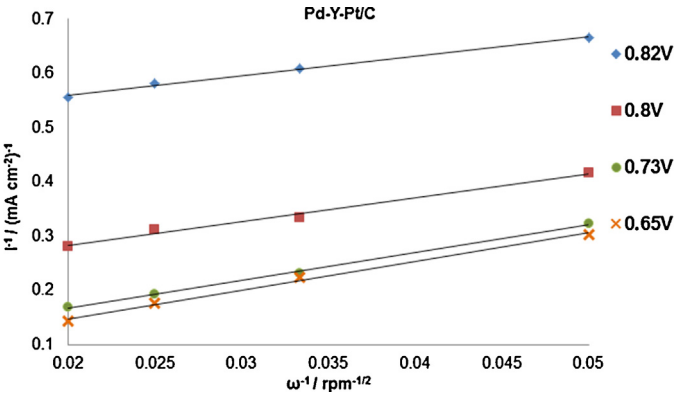

Fig. 9. Koutecky–Levich plots drawn from Fig. 8.

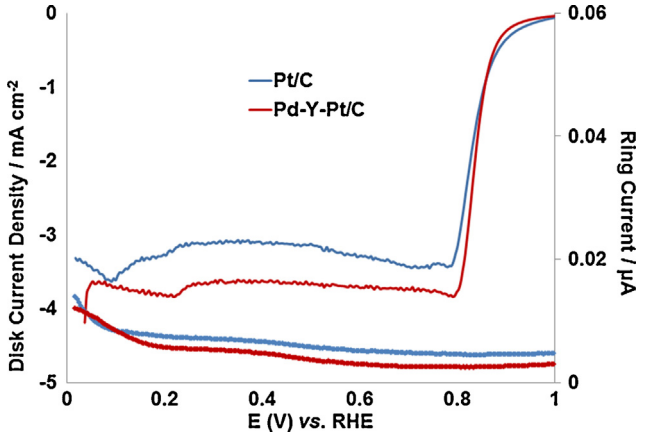

Fig. 10. Disk/ring response obtained by RRDE at 900 rpm for Pd–Y–Pt/C and Pt/C catalysts.

With the same catalyst loading on the GC electrode, metal mass activity is related to the particle size. Increased mass activity of core–shell catalysts are observed when compare to Pt/C catalyst. These can explain the reason that the core–shell structure catalysts have improved activity, as the catalytic activity is largely related to the active surface area. This trend is in agreement with the ECSA results, but in discrepancy with the TEM average particle size measurement. As discussed previously, controlled surface reaction preparation results in highly amorphous surface of the add-on metal and increase the surface area of the catalyst [15,31–33]. Same to EPSA, Pt mass activity of the core–shell catalysts was largely increased due to the benefit from the novel structure which reduces Pt amount.

The electrochemical oxygen reduction on Pt/C catalyst is known to occur in a four-electron transfer process [34,35]. Rotating ring disc electrode (RRDE) test, which confirms the catalyst's ORR activity was also performed. Results in Fig. 10 were obtained for Pd–Y–Pt/C catalyst and the disk/ring response obtained by RRDE at a constant rotation speed is compared with those of Pt/C catalyst. Such measurement was carried out by setting the potential of the ring electrode at 1.2 V, where the complete oxidation of H_2O_2 formed by oxygen reduction on the disc electrode was under diffusion controlled process. The percentages of peroxide generation at 0.4 V were calculated using the following equation based on the ring current:

$$\%H_2O_2 = 2 \times (I_R/N)/I_D + I_R/N$$

where I_R is ring current, I_D is disc current, and N is the collection efficiency coefficient which is 37%. The yield of H_2O_2 produced during ORR obtained at 900 rpm with 5 mV s^{-1} scan rate of Pd–Y–Pd/C

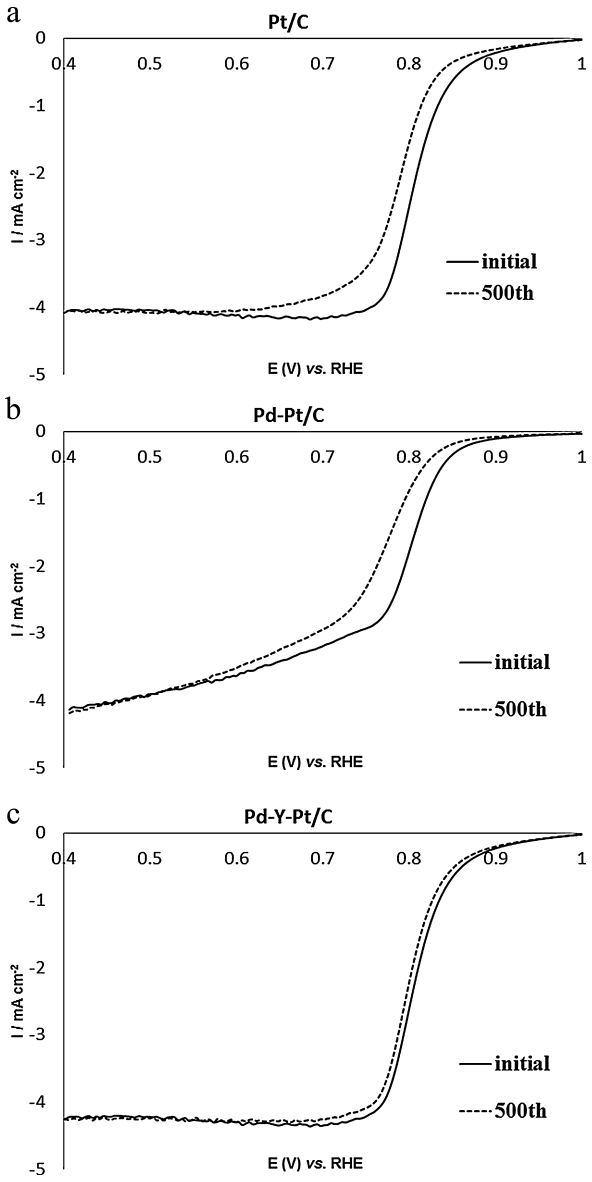

Fig. 11. Initial and the 500th scan of ORR ADT LSV of Pt/C, Pd–Pt/C and Pd–Y–Pt/C catalysts.

and Pt/C were 2.0% and 3.8%, respectively. This result suggested that Pd–Y–Pt/C showed higher activity and more 4-electron transfer process than Pt/C. The Pt/C activity obtained in this study was in agreement with the author's work on showing less than 4% H_2O_2 produced on Pt/C in 0.5 M H_2SO_4 [28,36]. This ORR activity improvement of Pd–Y–Pt/C catalyst is in agreement with Greeley's numerical research on ORR activity of Y, Pt and Pd catalysts [9].

To examine the stability of the catalyst in ORR conditions, the ADT test was carried out using RDE electrode after the ORR LSV tests in O_2 saturated 0.5 M H_2SO_4 (O_2 constant flushing). The rotation speed was kept at 900 rpm, the electrode was cycled from 1.0 to 0.4 V *vs.* RHE for 500 times at a scan rate of 5 mV s^{-1}. Fig. 11 shows the initial and the 500th scans of ORR ADT LSV of Pt/C, Pd–Pt/C and Pd–Y–Pt/C catalysts. Shifts on ORR onset potential toward negative direction was observed for all catalysts. It is noticeable that Pd–Y–Pt/C showed the smallest decrease and Pd–Pt/C showed the biggest. The shift of onset potential for Pt/C, Pd–Pt/C and Pd–Y–Pt/C were around 0.023 V, 0.021 V and 0.003 V, respectively. As detailed previously, Pt surface structure rearrangement happens at higher potential; the scan rate is slow enough for Pt sintering at these

potentials; bonding and debonding process between oxygen and catalyst may also accelerate this aspect. These 'damaged' the Pt/C giving a more negatively shifted onset ORR potential. The high durability of Pd–Y–Pt/C can be understood as the Y middle layer created approximately half filled metal–metal d bond between Pt (or Pd) and Y, this can be explained as the bonding states are filled and the antibonding states are empty [37]. Result indicated that, with the addition of Y, the Pd–Y–Pt/C has better durability in during the ORR. The Pd core is also protected by Y during ADT.

4. Conclusions

Pd–Y–Pt/C catalyst with core–shell–shell structure was synthesized using a controlled surface reaction method for ORR. This preparation method can create atomic layers of second and third metals on the surface of core material. The use of shell material is also dramatically reduced while the ORR activity was slightly increased. Meanwhile, the reduction of zero-valent Y was successful, there is no Y_xO_y detected even after exposing the catalyst to air. Y was most likely covered by the outer layer of Pt which protects the Y from contact with oxygen. Y, again, is a protection shell for Pd which is unstable during half cell testing. In half cell testing, the Pd–Y–Pd/C catalysts showed improved activity and durability compared to Pt/C and Pd–Pt/C core–shell catalyst. It showed comparable performance to 20% Pt/C with less than 7% of Pt in the catalyst. Therefore, core–shell–shell structure Pd–Y–Pt/C catalysts are a promising catalyst for low temperature and intermediate temperature PEM fuel cells.

Acknowledgements

We would like to thank EPSRC (project reference number EP/I037024/1) for the financial support; and LEMAS center for HRTEM/EDX analysis.

References

[1] M. Liu, C. Wang, F. Xie, Z. Mao, Int. J. Hydrogen Energy 38 (2013) 11011–11016.
[2] S. Mu, C. Xu, Y. Gao, H. Tang, M. Pan, Int. J. Hydrogen Energy 35 (2010) 2872–2876.
[3] E.H. Yu, X. Wang, X.T. Liu, L. Li, Catalysts for alcohol-fuelled direct oxidation fuel cells, Roy. Soc. Chem. (2012) 227–249.
[4] B. Avasarala, P. Haldar, Energy 57 (2013) 545–553.
[5] X.-Z. Yuan, H. Li, S. Zhang, J. Martin, H. Wang, J. Power Sources 196 (2011) 9107–9116.
[6] E. Antolini, Appl. Catal. B: Environ. 88 (2009) 1–24.
[7] J. Solla-Gullón, A. Rodes, V. Montiel, A. Aldaz, J. Clavilier, J. Electroanal. Chem. 554–555 (2003) 273–284.
[8] M.K. Jeon, P.J. McGinn, J. Power Sources 196 (2011) 1127–1131.
[9] J. Greeley, I.E.L. Stephens, A.S. Bondarenko, T.P. Johansson, H.A. Hansen, T.F. Jaramillo, J. Rossmeisl, I. Chorkendorff, J.K. Nørskov, Nat. Chem. 1 (2009) 552–556.
[10] T. Maiyalagan, K. Scott, J. Power Sources 195 (2010) 5246–5251.
[11] S. Limpattayanate, M. Hunsom, Renew. Energy 63 (2014) 205–211.
[12] L. Zhang, K. Lee, J. Zhang, Electrochim. Acta 52 (2007) 3088–3094.
[13] M.H. Seo, S.M. Choi, J.K. Seo, S.H. Noh, W.B. Kim, B. Han, Appl. Catal. B: Environ. 129 (2013) 163–171.
[14] K. Sasaki, J.X. Wang, H. Naohara, N. Marinkovic, K. More, H. Inada, R.R. Adzic, Electrochim. Acta 55 (2010) 2645–2652.
[15] E.M. Crabb, R. Marshall, Appl. Catal. A: Gen. 217 (2001) 41–53.
[16] A. Rose, E.M. Crabb, Y. Qian, M.K. Ravikumar, P.P. Wells, R.J.K. Wiltshire, J. Yao, R. Bilsborrow, F. Mosselmans, A.E. Russell, Electrochim. Acta 52 (2007) 5556–5564.
[17] M.A. Aramendía, V. Borau, C. Jiménez, J.M. Marinas, A. Moreno, Colloid Surf. A: Physicochem. Eng. Asp. 106 (1996) 161–165.
[18] S. Narayanan, K. Krishna, Catal. Today 49 (1999) 57–63.
[19] E.M. Crabb, M.K. Ravikumar, Electrochim. Acta 46 (2001) 1033–1041.
[20] B. Hammer, J.K. Nørskov, Surf. Sci. 343 (1995) 211–220.
[21] I.G. Casella, M. Contursi, J. Electroanal. Chem. 588 (2006) 147–154.
[22] M. Wakisaka, S. Mitsui, Y. Hirose, K. Kawashima, H. Uchida, M. Watanabe, J. Phys. Chem. B 110 (2006) 23489–23496.
[23] J.F. Moulder, W.F. Stickle, P.E. Sobol, K.D. Bomben (Eds.), Handbook of X-ray Photoelectron Spectroscopy, electronic ed., Eden Praire, 1995.
[24] S.M. Choi, M.H. Seo, H.J. Kim, W.B. Kim, Synth. Met. 161 (2011) 2405–2411.
[25] A.B.A.A. Nassr, A. Quetschke, E. Koslowski, M. Bron, Electrochim. Acta 102 (2013) 202–211.
[26] J. Zhao, A. Sarkar, A. Manthiram, Electrochim. Acta 55 (2010) 1756–1765.
[27] T. Maiyalagan, A.B.A. Nassr, T.O. Alaje, M. Bron, K. Scott, J. Power Sources 211 (2012) 147–153.
[28] S.M. Senthil Kumar, J. Soler Herrero, S. Irusta, K. Scott, J. Electroanal. Chem. 647 (2010) 211–221.
[29] G. Zhang, Z.-G. Shao, W. Lu, F. Xie, H. Xiao, X. Qin, B. Yi, Appl. Catal. B: Environ. 132–133 (2013) 183–194.
[30] N.A. Anastasijević, V. Vesović, R.R. Adžić, J. Electroanal. Chem. Interfacial Electrochem. 229 (1987) 305–316.
[31] S.K. Jain, E.M. Crabb, L.E. Smart, D. Thompsett, A.M. Steele, Appl. Catal. B: Environ. 89 (2009) 349–355.
[32] R. Burch, E.M. Crabb, Appl. Catal. A: Gen. 100 (1993) 111–130.
[33] B. Coq, E. Crabb, M. Warawdekar, G.C. Bond, J.C. Slaa, S. Galvagno, L. Mercadante, J.G. Ruiz, M.C. Sanchez Sierra, J. Mol. Catal. 92 (1994) 107–121.
[34] K. Ke, T. Hatanaka, Y. Morimoto, Electrochim. Acta 56 (2011) 2098–2104.
[35] L. Zhang, H. Li, J. Zhang, J. Power Sources 255 (2014) 242–250.
[36] V. Stamenković, T.J. Schmidt, P.N. Ross, N.M. Marković, J. Phys. Chem. B 106 (2002) 11970–11979.
[37] A.V. Ruban, H.L. Skriver, J.K. Nørskov, Phys. Rev. Lett. 80 (1998) 1240–1243.